

## Worcester Polytechnic Institute Digital WPI

---

Major Qualifying Projects (All Years)

Major Qualifying Projects

---

May 2011

# TMS Coil Design

Yi-Yu Tsai

*Worcester Polytechnic Institute*

Follow this and additional works at: <https://digitalcommons.wpi.edu/mqp-all>

---

### Repository Citation

Tsai, Y. (2011). *TMS Coil Design*. Retrieved from <https://digitalcommons.wpi.edu/mqp-all/3959>

This Unrestricted is brought to you for free and open access by the Major Qualifying Projects at Digital WPI. It has been accepted for inclusion in Major Qualifying Projects (All Years) by an authorized administrator of Digital WPI. For more information, please contact [digitalwpi@wpi.edu](mailto:digitalwpi@wpi.edu).

# TMS Coil Design

A Major Qualifying Project Report:  
Submitted to the Faculty  
of the



WORCESTER POLYTECHNIC INSTITUTE  
in partial fulfillment of the requirements for the  
Degree of Bachelor of Science

By:

---

**Yi-Yu Tsai**

Date: May 10, 2011

Approved by:

---

Professor Sergey Makarov, Project Advisor

## Table of Contents

General.....	3
TMS Coil .....	3
Power Consumption of TMS .....	5
What is <i>Maxwell</i> ?.....	7
Maxwell Modeling Process.....	7
Define Boundary Conditions .....	8
My Coil Designs .....	11
Case1 (O-shape coil with smaller diameter).....	11
Case2 (8-shape coil with opposite current directions).....	13
Case3 (8-shape coil with same current directions).....	15
Case4 (O-shape coil with doubled diameter).....	17
Coil Comparison and Comparison Results.....	19
Conclusion .....	20
References.....	21
Appendix A.....	23
Appendix B.....	27

# Section I

---

## **General**

Transcranial Magnet Stimulator (TMS) is a tool for the study of the human brain as well as a medical agent in psychiatry and neurology. TMS stimulate the brain by sending a pulsed current through a coil which produces a magnetic field that induces electric field in the brain and cause neurons to fire.

Current TMS techniques mostly stimulate the area of the brain close to its surface (less than 1cm in depth), the intensity of the electric field decrease as the distance increase. In order to stimulate deeper brain region, a very high intensity magnetic field would be needed. The intensity of the magnetic field cannot be satisfied by the standard magnetic stimulator designs such as circular coils. The double-cone coil is one of the coil designs that is able to create greater electrical field intensity and consider being the best tool for stimulation of deeper brain regions compare with other coil designs.

## **TMS Coil**

Electrical field intensity in the tissue and the rate of decrease of electrical field as function of distance from the coil, depend strongly on the orientation of coil elements relative to tissue surface. Physiology studies indicate that optimal activation occurs when field is oriented in the same direction as the nerve fiber. Therefore, In order to stimulate deep brain regions, it's necessary to use coils in orientations that they will produce a significant field in the preferable direction to active the neuronal structures or axons.

The construction of H coil should meet the following 3 goals

1. High enough electric field intensity in the desired deep brain region that will surpass the threshold for neuronal activation.
2. High percentage of electric field in the desired deep brain region relative to maximal intensity in the cortex
3. Minimal side effects such as pain and activation of facial muscles.

The geometrical features of each specific design are mainly dependent on two goals:

1. The location and size of the deep brain region or regions intended to be activated
2. The preferred direction or directions of stimulation.

Even though the specific designs look different, all the H-coil share the following features

1. *Base complementary to the human head.* This feature guarantees that all the wires in the base will be tangential to the head. This configuration maximizes both the intensity and the penetration depth of the electric field induced by the base in the brain.
2. *Proper orientation of stimulating coil elements.* Coils must be oriented such that they will produce a considerable field in a direction tangential to the surface, which should also be the preferable direction to activate the neuronal structures under consideration.
3. *Summation of electric impulses.* The induced electric field in the desired deep brain regions is obtained by optimal summation of electric fields, induced by several coil elements with common direction, in different locations around the skull
4. *Minimization of nontangential components.* The length of coil elements which are not tangential to the brain tissue surface should be minimized. Furthermore, the nontangential

coil elements should be as small as possible and placed as far as possible from the deep region to be activated.

5. *Remote location of return paths.* The wires leading currents in a direction opposite to the preferred direction (the return paths) should be located far from the base and the desired brain region. This enables a higher absolute electric field in the desired brain region. In some cases, the return paths may be in the air. In other cases, part of the return paths may be adjacent to a different region in the head which is distant from the desired brain region.
6. *Shielding.* Since the return paths are far from the main base, it is possible to screen all or part of their field by inserting a shield around them or between them and the base. The shield is comprised of a material with high magnetic permeability, capable of inhibiting or diverting a magnetic field, such as mu-metal, iron or steel core. Alternatively, the shield is comprised of a metal with high conductivity which can cause electric currents or charge accumulation that may oppose the effect produced by the return portions.

## **Power Consumption of TMS**

The pulse width (PW) of the TMS device is the key to enables response characterization of different neuronal populations. However the conventional TMS cannot control the pulse width (PW) due to the limitation of the switching device (SCR) that can only be turned off when the anode current reaches zero. As the technology improved and high quality switch coming to the market, PW limitation no longer exist since the introduction of the cTMS (TMS with controllable pulse width) in 2008. The new design not only reduces the power consumption but also reduces the coil heating due to its near-rectangular pulse.

The basic circuit of cTMS is similar to the conventional TMS stimulator with the main difference that the switch is implemented with a semiconductor device that can be turned off from the gate terminal. The switch connects the stimulating coil to the energy-storage capacitor. When the switch is ON, the current in the capacitor will flow through the coil. The increment of the approximately linear current in the coil will induce near rectangular electric field pulse into the brain proportional to the coil current rate of change. When the switch is OFF, the current in the coil will discharge through the freewheeling diode and the dissipation resistor across the coil. The PW of the device is limited to a quarter resonant periods that corresponds to complete discharge of the capacitor. The device controller will control the voltage of capacitor through the charger and also control the PW by triggering the switch ON/OFF time. The snubber is needed in this device in order to prevent the large voltage spikes that can damage the semiconductor component and also prevent the power loss when the switch is OFF.

# Section II

---

## **What is *Maxwell*?**

*Maxwell* is the electromagnetic field simulation software for designing and analyzing that uses finite element analysis to solve three-dimension electric, magnetostatic, eddy current and transient problem. *Maxwell* is one of the few products created by the company named Ansys/Ansoft. HFSS is another well known Ansoft product for simulation of high frequency applications such as antenna. Both Maxwell and HFSS have very similar user interface and set ups which means designer with Maxwell background will get use to HFSS in a very short time vice versa.

## **Maxwell Modeling Process**

The modeling process is demonstrated in the following steps:

1. Create a new project and insert a *Maxwell* design. Based on the application choose the solution type of electromagnetic analysis to be performed for example: magnetostatic.
2. Draw the geometry of the model using the drawing space provided by the 3D Modeler menu. Use the Drawing tools that locate above the Modeler menu. Be aware to assign variables to the position and the XYZ size of the objects. The reason behind this step is to keep track of all design objects; it's very common to change the size or location of the objects during the design process.
3. Assign the material properties to all solid objects in the model for example: copper. Define new material properties if materials in the default library do not exist.



4. Specify the field sources (excitations) for the solution. The excitation can represent by a 2D rectangle or a circle that locate with in the design object such as a wire.
5. Specify the boundary conditions for the solution. Boundary condition is usually represented by a box that tells the simulation when to stop calculating. More detail on boundary conditions will discuss on the next part.
6. Define the additional global parameters to calculate such as magnetic field.
7. Define mesh operations for special applications.
8. Specify solution options
9. Start the solution process
10. Calculation time for the solution range from an hour to days depend on how complex the design and how accurate for the design. Therefore it's important to manage the running time. Result such as plotting field quantities and calculating expressions will be ready.

## **Define Boundary Conditions**

Boundary conditions are fundamental to solution of *Maxwell's* equations that enable one to control the characteristics of interfaces between objects. The field equations that are solved by Maxwell are derived from the differential form of *Maxwell's* Equations. For these expressions to be valid, it is assumed that the field vectors are single-valued, bounded, and have continuous distribution along with their derivatives. Along boundaries, the fields are discontinuous and the derivatives have no meaning. Therefore boundary conditions define the field behavior across discontinuous boundaries. Since boundary conditions force a field behavior, make sure the assumptions are appropriate for the simulation. Improper use of boundary conditions may lead to inconsistent results. Boundary conditions can be utilized to reduce the model complexity. Unlike

the real world that is bounded by infinite space, the simulation needs to be made finite. In order to achieve this finite space, *Maxwell* applies an *outer boundary* condition which is applied to the region surrounding the geometric model. The model complexity is directly related to the solution time and computer resources so it is an advantage to utilize proper boundary conditions for any model.

The default boundary conditions for the *Maxwell* Magnetostatic solver are Natural boundaries on the interface between objects and Neumann boundaries on the outer boundaries. Natural boundary means that the H Field is continuous across the boundary. Neumann boundary means that the H Field is tangential to the boundary and flux cannot cross it. The default boundary conditions are used to model ordinary field behavior. Initially, object interfaces are natural boundaries; outer boundaries and excluded objects are Neumann boundaries.

Surface Approximations boundaries include Symmetry Planes, Perfect E or Perfect H. Perfect F is a perfect electrical conductor, also referred to as a perfect conductor. This type of boundary forces the electrical field perpendicular to the surface. Perfect H is a perfect magnetic conductor; Forces E-field tangential to the surface.

Symmetry Boundary represents perfect E or perfect H planes of symmetry. Fields behave as Odd Symmetry (Flux Tangential) or Even Symmetry (Flux Normal). Odd Symmetry, H is tangential to boundary; its normal components are zero. Even Symmetry, H is normal to the boundary; its tangential components are zero. Zero Tangential H Field boundaries are often used to model an applied uniform, external field. This would model outer boundaries of the Region that are perpendicular to the applied field. In this case, the boundary should be placed far from the structure so that the simulation is not over-defined. Symmetry boundaries as opposed to a

simple Perfect E or Perfect H should be used when the plane cuts across a port. More detail equations of boundary conditions are including in Appendix A and Appendix B.

# Section III

---

## My Coil Designs

### Case1 (O-shape coil with smaller diameter)

Solution set up to “15Maximun Number of Passes” and the “Percent error of 1e-6”

Material of the coils is copper

The inner-radius of the coil is 27.25mm

The outer-radius of the coil is 42.25mm

The height of the coil is 10mm

The current excitation value is 1000A

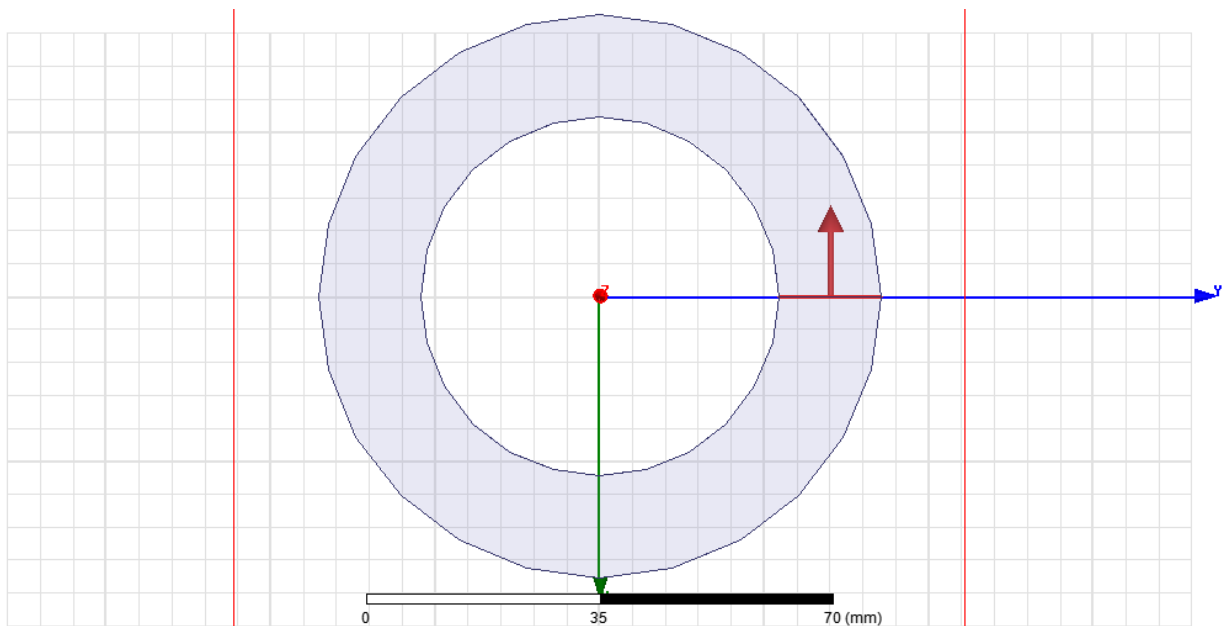


Figure1. Current excitations

Figure 2 shows the magnetic field contour plot for YZ plane. The magnetic field magnitude 20mm below center of coil is  $5.57 \times 10^3$  A/m.

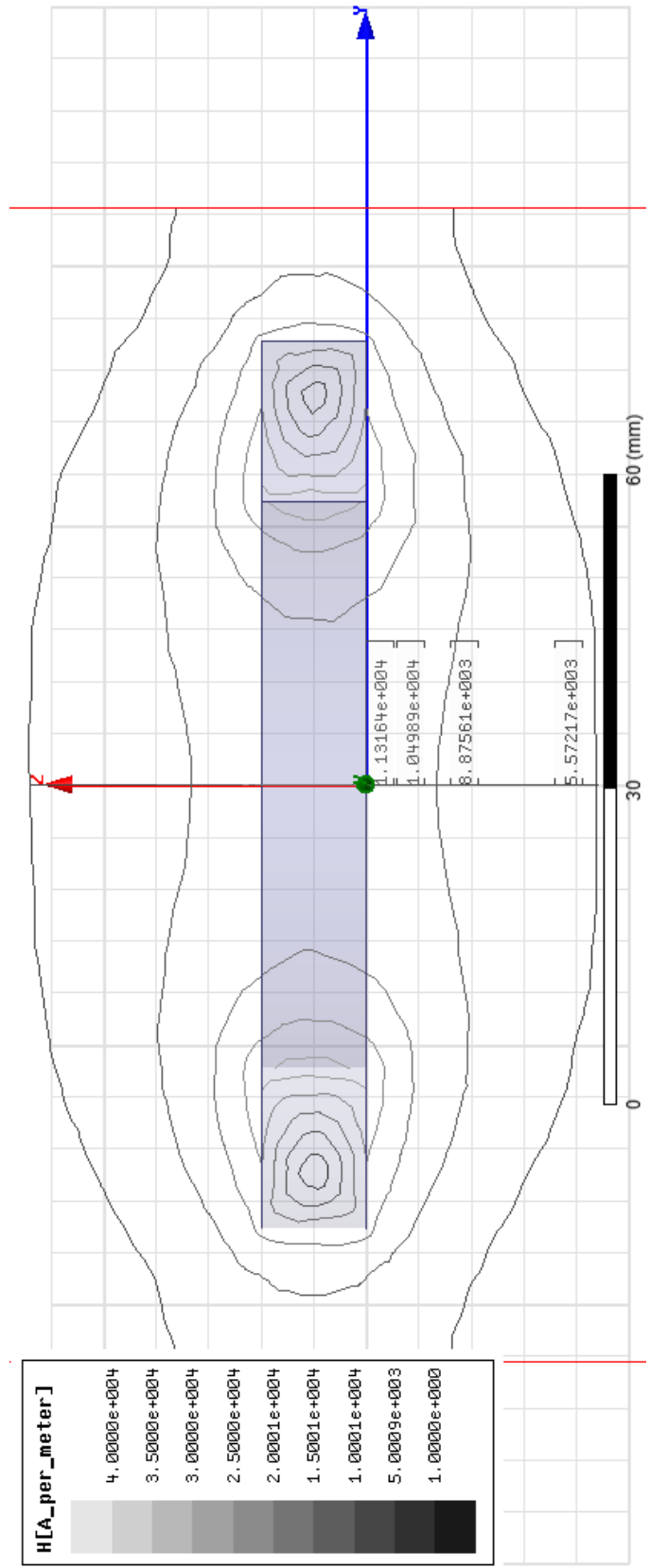


Figure2. Magnetic Field Contour Plot for YZ plane

## Case2 (8-shape coil with opposite current directions)

Solution set up to “15Maximun Number of Passes” and the “Percent error of 1e-6”

Material of the coils is copper

The inner-radius of the coil is 27.25mm

The outer-radius of the coil is 42.25mm

The height of the coil is 10mm

The current excitation value is 1000A

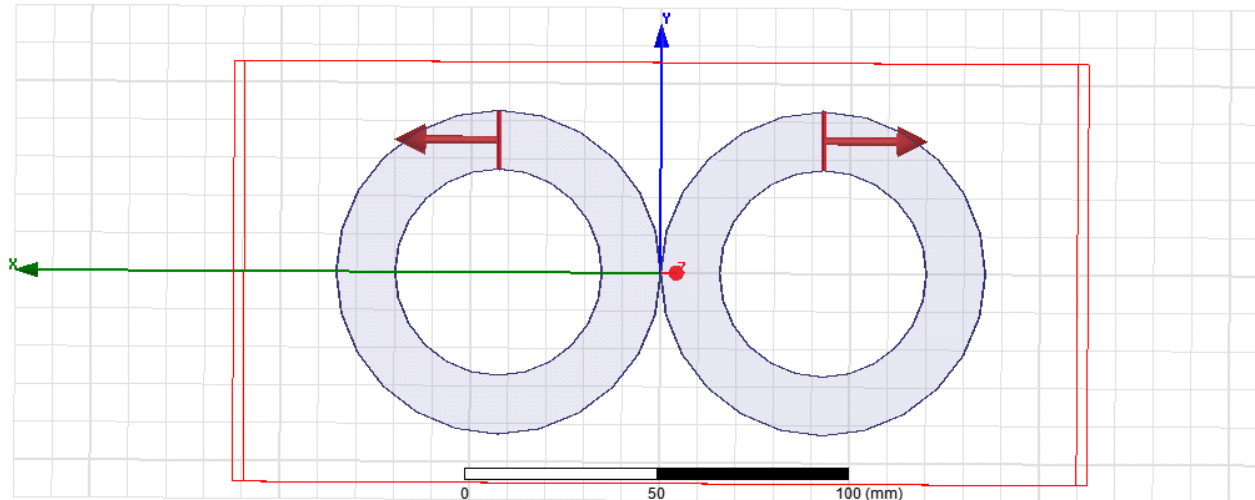


Figure3. Current excitations

Figure 4 shows the magnetic field contour plot for YZ plane. The magnetic field magnitude 20mm below center of coil is  $8.48 \times 10^3$  A/m.

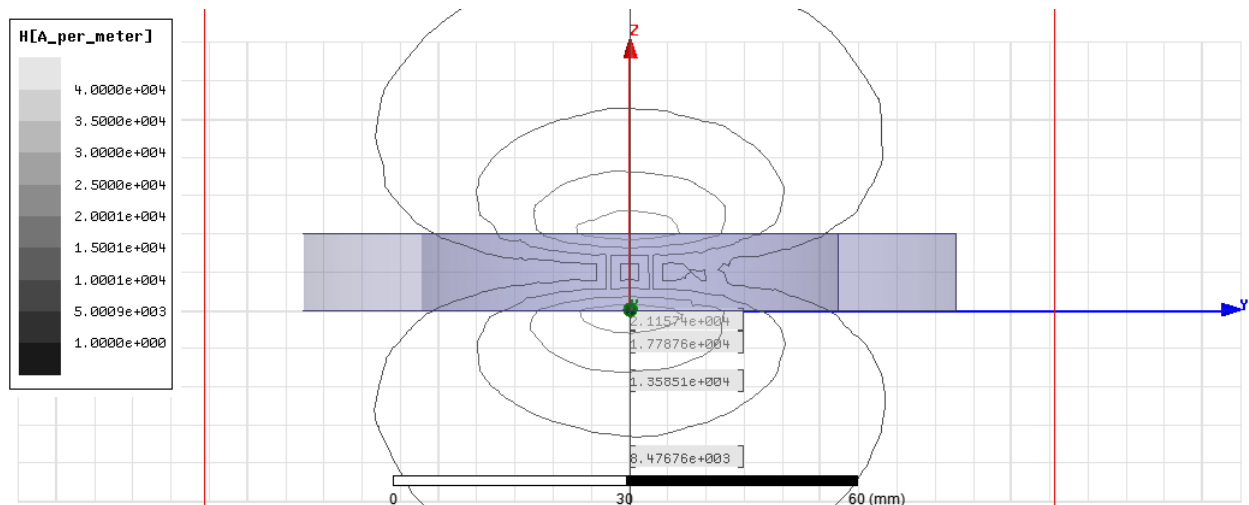


Figure4. Magnetic Field Contour Plot for YZ plane

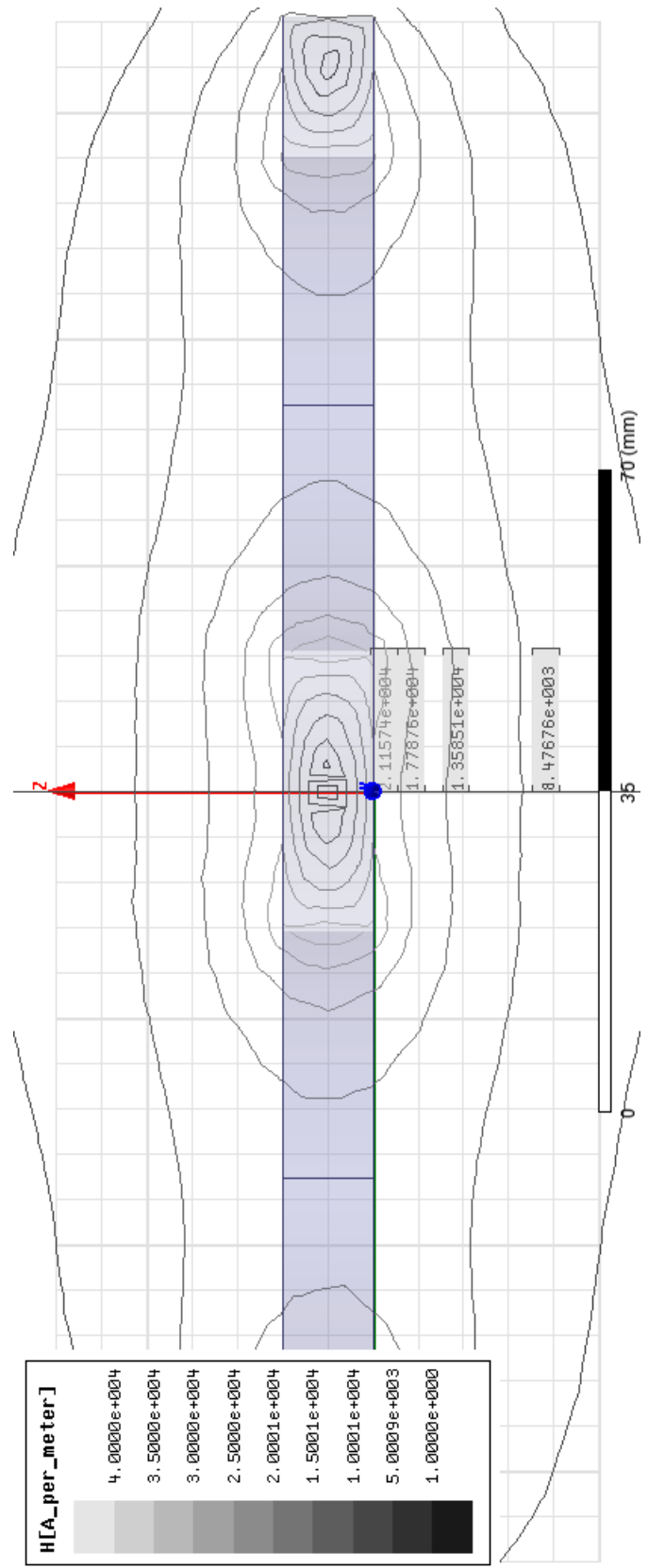


Figure5. Magnetic Field Contour Plot for XZ plane

### Case3 (8-shape coil with same current directions)

Solution set up to “15Maximum Number of Passes” and the “Percent error of 1e-6”

Material of the coils is copper

The inner-radius of the coil is 27.25mm

The outer-radius of the coil is 42.25mm

The height of the coil is 10mm

The current excitation value is 1000A

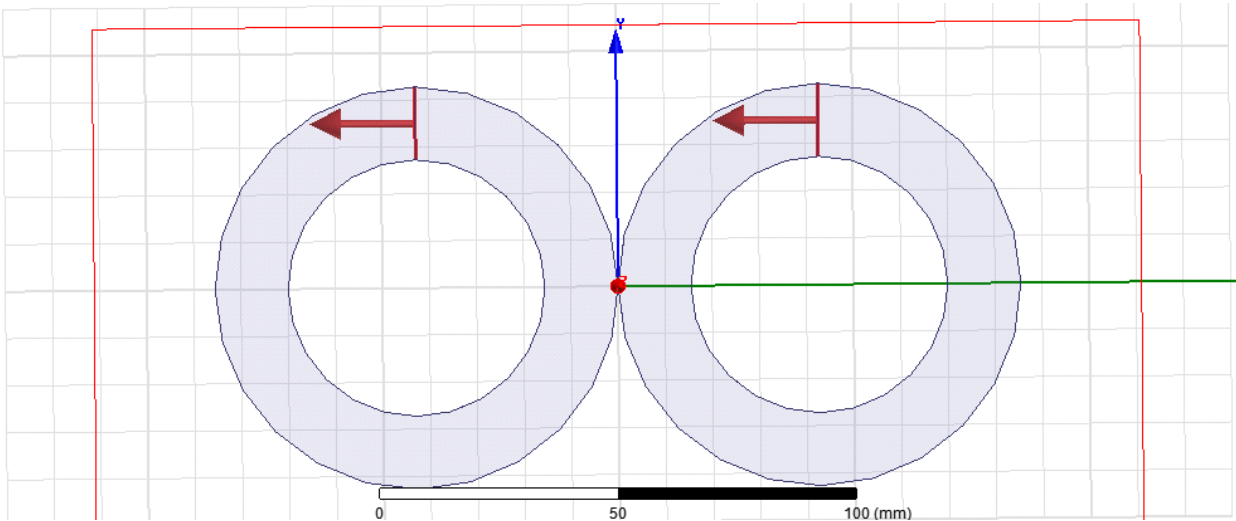


Figure6. Current excitations

Figure 7 shows the magnetic field contour plot for YZ plane. The magnetic field magnitude 20mm below center of coil is  $5.69 \times 10^2$  A/m.

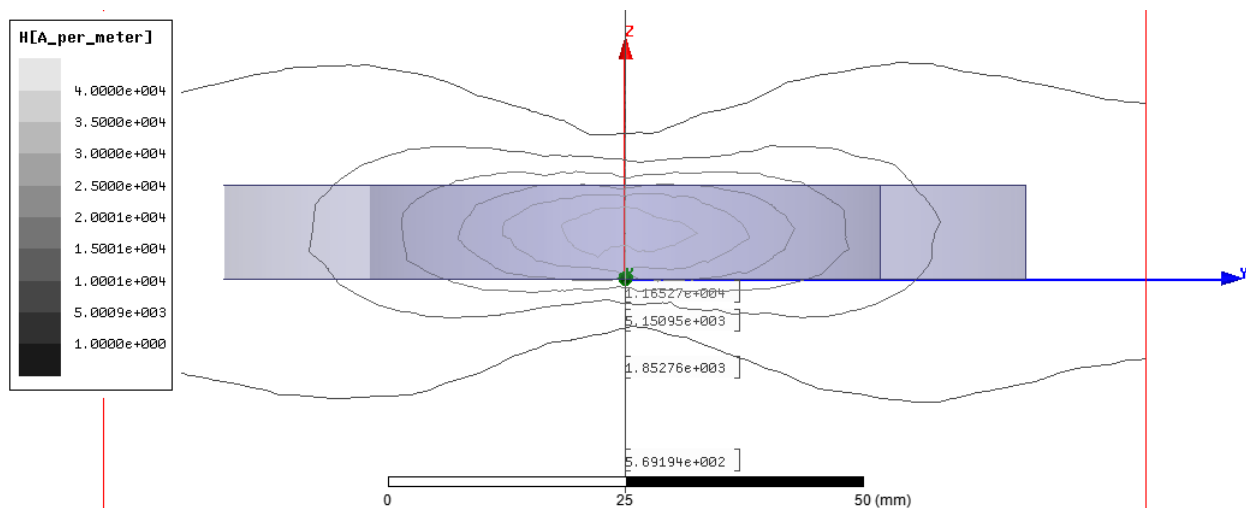


Figure7. Magnetic Field Contour Plot for YZ plane



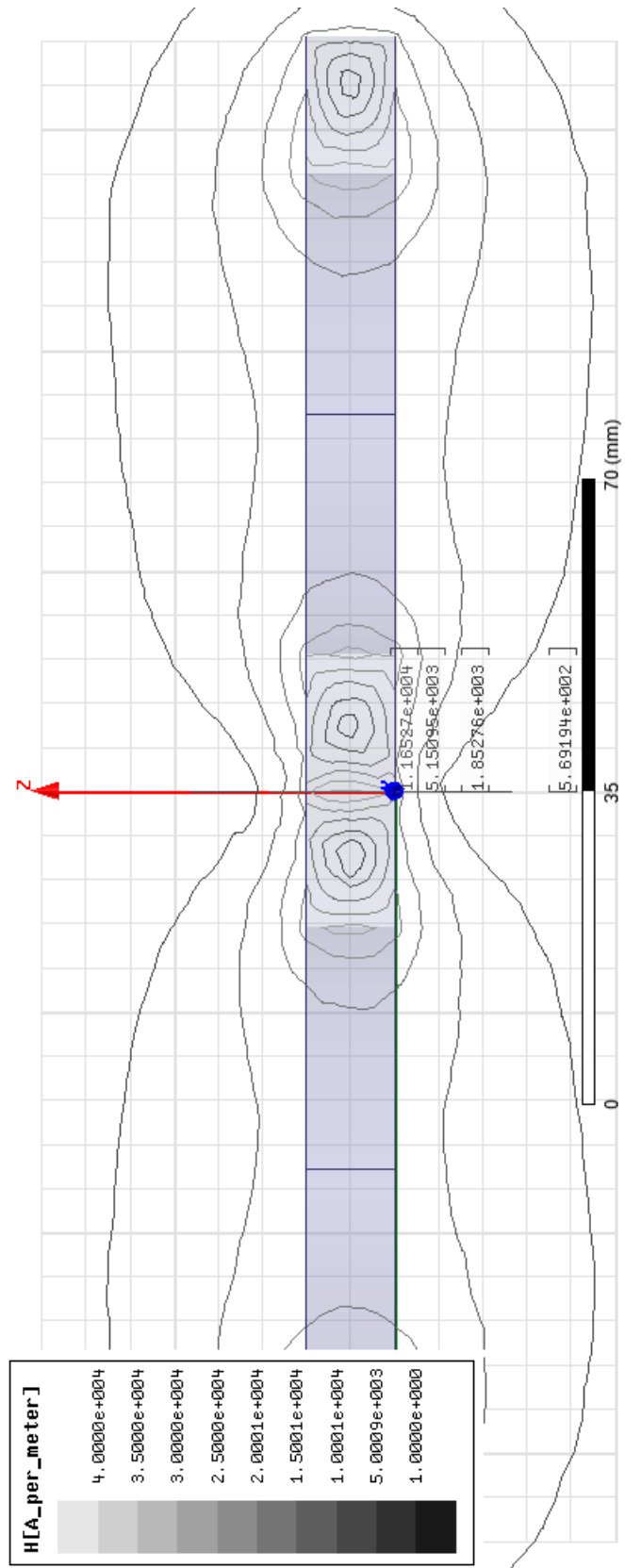


Figure8. Magnetic Field Contour Plot for XZ plane

#### Case4 (O-shape coil with doubled diameter)

Solution set up to “15Maximum Number of Passes” and the “Percent error of 1e-6”

Material of the coils is copper

The inner-radius of the coil is 62.25mm

The outer-radius of the coil is 77.25mm

The height of the coil is 10mm

The current excitation value is 1000A

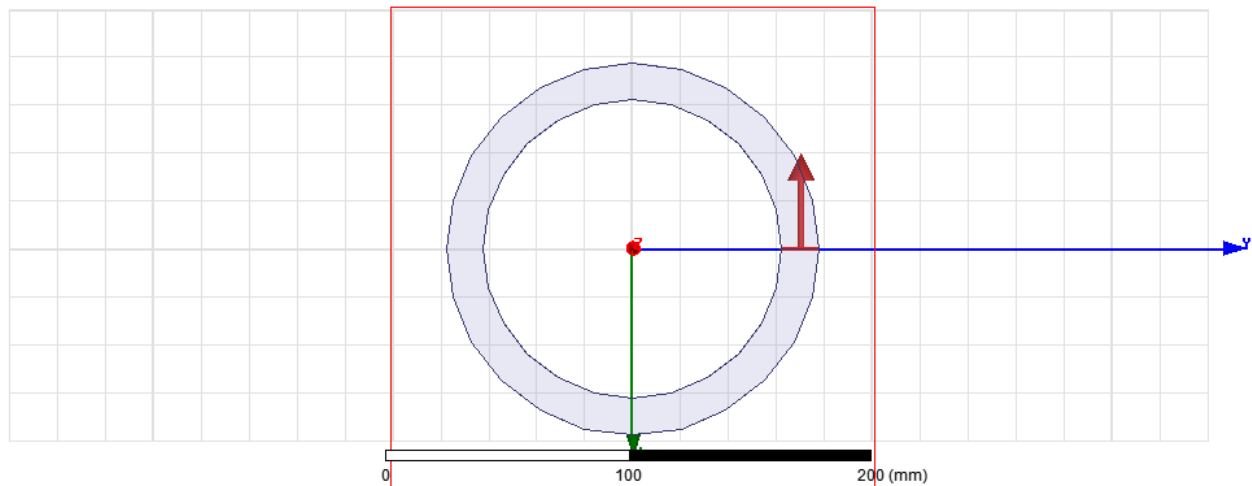


Figure9. Current excitations

Figure 10 shows the magnetic field contour plot for YZ plane. The magnetic field magnitude 20mm below center of coil is  $3.46 \times 10^3$  A/m.

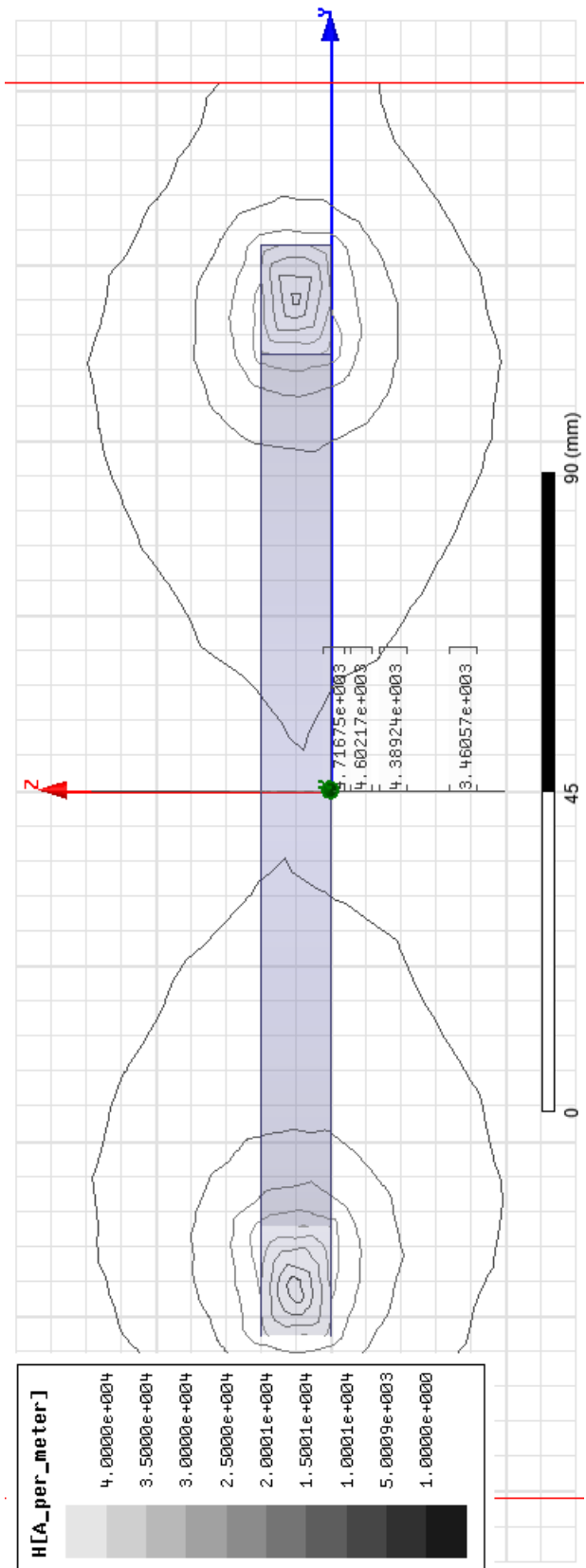
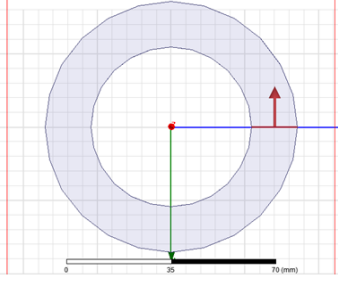
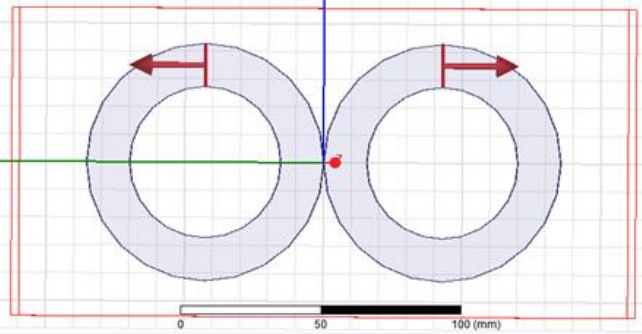
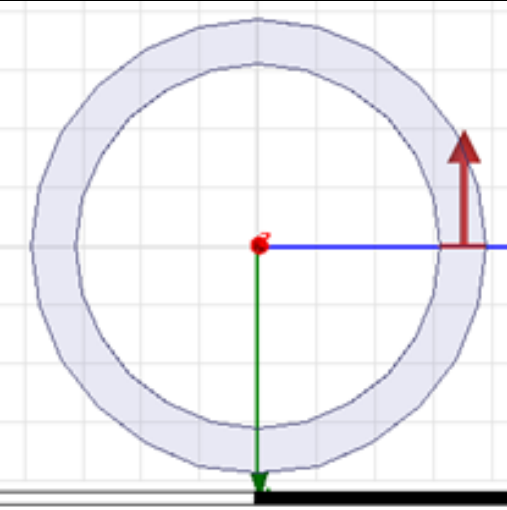
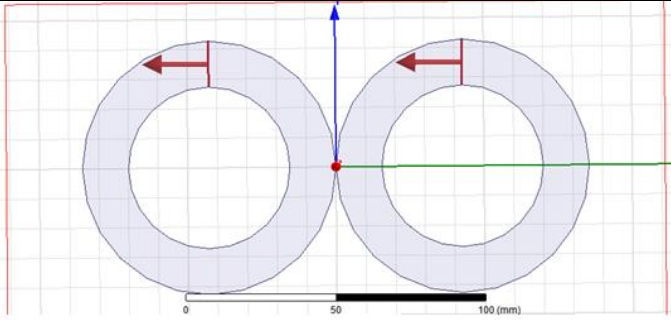


Figure10. Magnetic Field Contour Plot for YZ plane

## Coil Comparison and Comparison Results

The following table shows the comparison of the H field below the coil center all with current excitation 1000A. The magnetic field magnitude is found at the same depth (20mm) for four different coil designs.

Table1

	
<p>Radius=35mm, <math>H = 5.57 \cdot 10^3</math> A/m</p>	<p>Radius=35mm, <math>H = 8.48 \cdot 10^3</math> A/m</p>
	
<p>Radius=70mm, <math>H = 3.46 \cdot 10^3</math> A/m</p>	<p>Radius=35mm, <math>H = 5.69 \cdot 10^2</math> A/m</p>

## **Conclusion**

We can see that the O-shaped coil with 35mm radius has close to double magnetic field magnitude as compared to the O-shaped coil with 70mm radius. The 8-shaped coil with opposite current directions has magnetic field magnitude 15 times stronger than the 8-shaped coil with same current directions. As a result, the 8-shaped coil with opposite current directions has the strongest magnetic field magnitude among 4 different coil designs.

## References

- Al-Mutawaly, N. (2002). *A Novel Coil Design For Magnetic Nerve Stimulation*.
- Ansoft. (2006). Maxwell 3D Field Simulator v11 User's Guide.
- Hiwaki, O. (2008). *Modification of Motor Evoked Potentials Caused by Electrical Peripheral Nerve Stimulation in Transcranial Magnetic Stimulation*. IEEE Transactions on Magnetics.
- Kim, D.-H. (2006). *Improved Field Localization in Transcranial Magnetic Stimulation of the Brain With the Utilization of a Conductive Shield Plate in the Stimulator*. IEEE Transactions on Biomedical Engineering.
- LAKIĆ, D. (2006). *Calculation of Magnetic Flux Density Using Maxwell 3D*.
- Levkovitz, Y. (2007). *A randomized controlled feasibility and safety study of deep transcranial magnetic stimulation*.
- Lorrain, P. (1978). *Electromagnetism Principles and Applications*. San Francisco: W.H. Freeman and Company.
- Odagaki, M. (2008). *Suppression of Electromyogram of Hand Muscle Elicited by Transcranial Magnetic Stimulation Over the Primary Motor Cortex*. IEEE Transactions on Magnetics.
- Okabe, M. (1983). Effects of Magnetic Characteristics of Materials on the Iron Loss in the Three Phase Transformer Core. *IEEE Trans. Magn*, 2192-2194.
- Peterchev, A. V. (2008). *A Transcranial Magnetic Stimulator Inducing Near-Rectangular Pulses With Controllable Pulse Width (cTMS)*. *IEEE Transactions on Biomedical Engineering*.

- Roth, B. (1990). *A theoretical calculation of the electric field induced by magnetic stimulation of a peripheral nerve.*
- Roth, Y. (2002). A Coil Design for Transcranial Magnetic Stimulation of Deep Brain Regions. *Journal of Clinical Neurophysiology*, 361-370.
- Ruohonen, J. (2000). *Coil Design for Real and Sham Transcranial Magnetic Stimulation*. IEEE Transactions on Biomedical Engineering.
- Zangen, A. (2002). *Transcranial magnetic stimulation induces increases in extracellular levels of dopamine and glutamate in the nucleus accumbens.* NeuroReport.
- Zangen, A. (2005). Transcranial magnetic stimulation of deep brain regions: evidence for efficacy of the H-Coil. *Clinical Neurophysiology*, 775-779.
- Zhang, X. (2008). *Standed Core Transformer Loss Analysis*. Thesis.

## Appendix A

[http://www.phd.etfbl.net/files/Works\\_PDF/Lacic%20Dragoljub.pdf](http://www.phd.etfbl.net/files/Works_PDF/Lacic%20Dragoljub.pdf)

### CALCULATION OF MAGNETIC FLUX DENSITY USING Maxwell 3D VERSION 10

**Abstract:** Present knowledge limits magnitude of quantities of electrical and magnetic fields. This fact is also considered by government of many countries including BiH throughout law. So we must be prepared to offer solutions for actual construction sites that will be correspondent later to measurement upon finishing actual facilities. One way is to use existing software solutions.

#### INTRODUCTION

Problem that I was solving in this paper is a problem that I faced on my working place. I had to calculate current that will flow through a three phase cable that connects distribution cabinet and main switchgear cabinet of one building. My calculation determined value:

$$\begin{aligned}i_{L1}(t) &= 295 \cdot (\cos \omega \cdot t) [A] \\i_{L2}(t) &= 295 \cdot (\cos \omega \cdot t + 2\pi/3) [A] \\i_{L3}(t) &= 295 \cdot (\cos \omega \cdot t + 4\pi/3) [A]\end{aligned}\quad (1)$$

Position of cable is inside a building and near future working places. So my desire was to establish a value of magnetic flux density in a presence of human body, more exactly inside human body. Limits posed by law sets that value below  $100 T \mu$ .

#### MODELING

##### Description of software package

Maxwell 3D is an interactive package for analyzing electric and magnetic fields in three-dimensional structures. Software finite element based field solvers enable us to simulate electric and magnetic fields in any type of device. To represent an electrical or magnetic field over a large, irregularly-shaped region, Maxwell 3D divides the region into many tetrahedra – figure 1 (pyramid-shaped sub-regions).

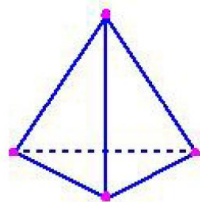


Fig. 1 - Tetrahedron

The collection of tetrahedral is referred to as the finite element mesh – or simpler, the mesh. To obtain a precise description of the field, the system must size each tetrahedron so that it is small enough for the field to be adequately



interpolated from the nodal values. The accuracy of the solution depends on how small each of the individual elements are. The optimal mesh for a structure is one that contains enough tetrahedral to accurately represent a field solution but not so many that the available computing resources are overwhelmed. Program can use three ways to make sure that tetrahedral are placed wisely: adaptive mesh refinement, manual mesh refinement and combination. I used first principle. During solution process, software iteratively refines the mesh in regions where error is high. This allows the simulator to target mesh refinement to the areas that need it, optimizing computing resources.

### Geometrical modelling and solving of problem

First we have to define geometrical bodies, that will represent cable and human body. Both models are placed in vacuum, and vacuum has similar properties as air. As a model of a cable I used three conductors, whose properties are set to represent copper. This is option which you can set inside a program.

Conductor is shaped as cylindrical object, with  $r = 5.5\text{mm}$ ,  $H = 5000\text{mm}$  that  $r$  represent radius of basis of cylinder and  $H$  represent height of conductor. This value is an approximation of a cable with a conductors that are used inside of building ( $4.95\text{mm}^2$ ). As I mentioned before, it is very easy to set properties in this simple case. The conductors are placed in close vicinity between each other. As you can notice there are no insulation on these conductors.

Body is also shaped as actual body. This form is combination of 4 different figures that are unite in one. Fig. 2 shows window for drawing geometrical bodies and my models represented in planes (2D) and space (3D).

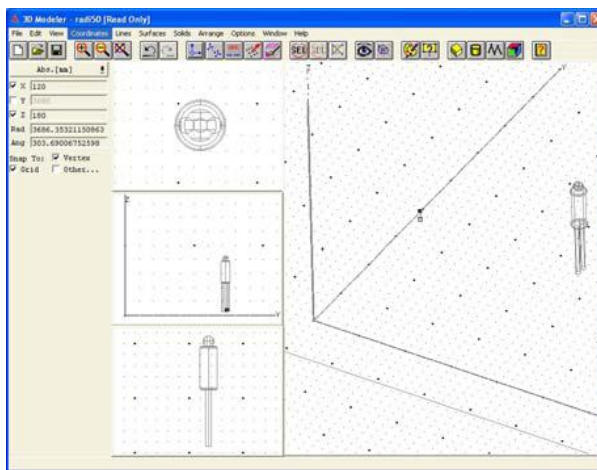


**Fig. 2** – Drawing of objects in 3D

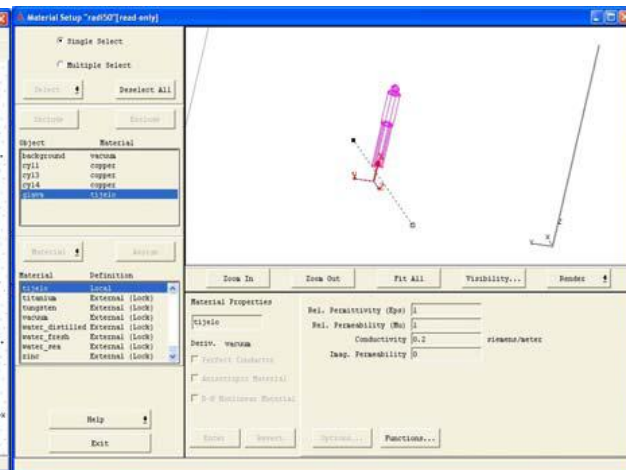


**Fig. 3-** Properties of object

Next step is to define sources or boundary conditions. Due to my problem, logical solution was to pick a source. At next figure, number 4, you can observe this.

With a finishing of this process, you can start a simulation. You can very easy set percent of refinement at each pass, a number of passes and percent error. I set per-cent error at 1%, but I achieved 5,2% after 10 passes. After 10 passes, he made around 134000 tetrahedra (Fig.5)

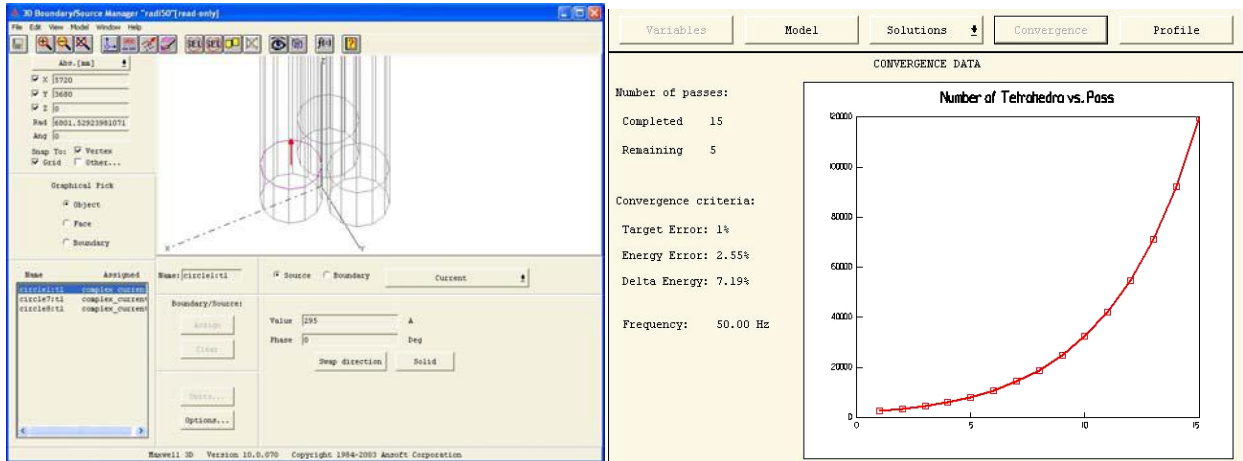


**Fig. 5** – Graph tetrahedra=f(number of pass)

Finally, results are obtained after approximately one hour from the beginning of simulation. They are represented at next figure (Fig.6).

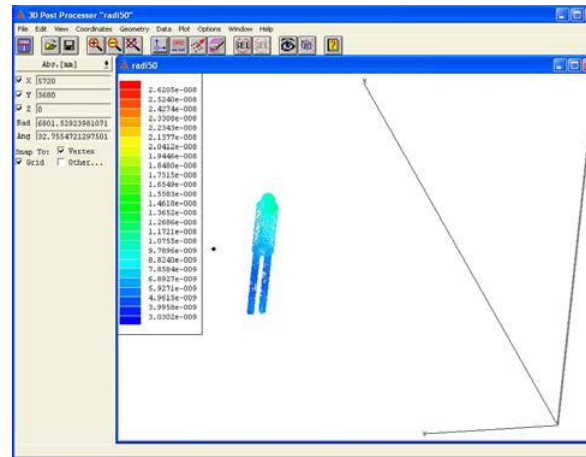


**Fig. 6 – Results of simulation**

As you can see, upper values are around  $0,018T\mu$ , and they are much below values that are concerning for human health.

Of course, main issue lays in fact that software is not with open source, so we must relay that a proper design of software lies behind our results. Also I used the simplest way to model cable and human body. But engineers are known as a people that tries to find the simplest solution.

## CONCLUSION

I tried in this simple way to show in the easiest way possible, through a picture in 3D way, how you can explain to others values of Magnetic flux density. Lawmakers in this region predicts possibility of calculation of quantities of fields, together with an actual measurement on sites. So we should encourage production of software packages with their academic background. Also these packages do not need to be large, and they could be formed as modules. This is a way how we can inside our universities make an enterprise that could benefit to everybody, from a young researchers that will be better paid to the needful economic income for development in a new environment.

## Appendix B

[http://archive.uky.edu/bitstream/10225/879/MS\\_Thesis\\_by\\_XingxingZhang.pdf](http://archive.uky.edu/bitstream/10225/879/MS_Thesis_by_XingxingZhang.pdf)

### Chapter 2. B-H curve Modification via Finite Element Method

In the process of 3D modeling using Maxwell 3D, uniform core is used to substitute stranded core. Therefore, the B-H curve which represents the material characteristics needs to be modified. In this chapter, a two-dimensional finite element approach is used to modify the B-H curve for uniform core.

#### 2.1 Theory and formulations

##### 2.1.1 Govern equation and weak form

The 2D magnetostatic problem has been formed in terms of the magnetic vector potential A, which defined as:

$$\nabla \times \vec{A} = \vec{B} \quad (2.1)$$

$$\nabla \cdot \vec{A} = 0 \quad (2.2)$$

It is assumed that the excitation  $J = J_z \hat{z}$  which is independent of the variable z. For this excitation, the vector potential  $\vec{A}$  has  $\hat{z}$  component only. The govern vector Poisson equation  $\vec{A}$  for can be written as:

$$\nabla \times \left( \frac{1}{\mu_r} \nabla \times \vec{A}_z \right) = \mu_0 \vec{J}_z \quad (2.3)$$

Therefore, the magnetic flux density can be calculated from  $\vec{B} = \nabla \times \vec{A}_z$  [11, 12]. In the above,  $\mu_r$  is the relative permeability which is a function of position.

Introducing a test function  $\vec{A}_z^a$ , we can derive the weak form of vector Poisson equation as,

$$F(\vec{A}_z, \vec{A}_z^a) = \int_V \vec{A}_z^a \cdot \left\{ \left[ \nabla \times \left( \frac{1}{\mu_r} \nabla \times \vec{A}_z \right) \right] - \mu_0 \vec{J}_z \right\} dV \quad (2.4)$$

Using vector identity  $\vec{A} \cdot \nabla \times \vec{B} = -\nabla \cdot (\vec{A} \times \vec{B}) + \vec{B} \cdot \nabla \times \vec{A}$ , Equation (2.4) can be simplified in a 2D case [11],

$$F(\vec{A}_z, \vec{A}_z^a) = \frac{1}{\mu_r} \int_V \nabla \times \vec{A}_z^a \cdot \nabla \times \vec{A}_z dV - \mu_0 \int_V \vec{A}_z^a \cdot \vec{J}_z dV - \frac{1}{\mu_r} \oint_{\Gamma} \vec{A}_z^a \times (\nabla \times \vec{A}_z) \cdot \hat{n} dl \quad (2.5)$$

where  $\hat{n}$  denotes the unit vector normal to  $\Gamma$ .

Equation (2.5) is the weak form of 2D vector Poisson equation.

##### 2.1.2 Triangular elements

Before the derivation of finite element analysis for a 2D magnetostatic problem, a useful area coordinates ( $L_1, L_2, L_3$ ) is presented below.

A convenient set of coordinates  $(L_1, L_2, L_3)$  for a triangle  $(1, 2, 3)$  Figure 2.1 is defined by the following linear equations in Cartesian system:

$$\begin{cases} x = L_1x_1 + L_2x_2 + L_3x_3 \\ y = L_1y_1 + L_2y_2 + L_3y_3 \\ 1 = L_1 + L_2 + L_3 \end{cases} \quad (2.6)$$

Every set of  $(L_1, L_2, L_3)$  corresponds to a unique set of Cartesian coordinates [13].  
Solving Equation (2.6) for  $x$  and  $y$ , we have

$$\begin{cases} L_1 = \frac{a_1 + b_1x + c_1y}{2\Delta} \\ L_2 = \frac{a_2 + b_2x + c_2y}{2\Delta} \\ L_3 = \frac{a_3 + b_3x + c_3y}{2\Delta} \end{cases} \quad (2.7)$$

where,

$$\Delta = \frac{1}{2} \det \begin{vmatrix} 1 & x_1 & y_1 \\ 1 & x_2 & y_2 \\ 1 & x_3 & y_3 \end{vmatrix} = \text{area of triangle 123}$$

and

$$\begin{cases} a_1 = x_2y_3 - x_3y_2 \\ b_1 = y_2 - y_3 \\ c_1 = x_3 - x_2 \end{cases} \quad (2.8)$$

$$\begin{cases} a_2 = x_3y_1 - y_3x_1 \\ b_2 = y_3 - y_1 \\ c_2 = x_1 - x_3 \end{cases} \quad (2.9)$$

$$\begin{cases} a_3 = x_1y_2 - y_1x_2 \\ b_3 = y_1 - y_2 \\ c_3 = x_2 - x_1 \end{cases} \quad (2.10)$$

Based on the above definition, we observe that when point  $P$  on edge 23,  $L_1 = 0$ ; if it is on vertex 1, then  $L_1 = 1$ .

When point  $P$  on edge 13,  $L_2 = 0$ ; if it is on vertex 2, then  $L_2 = 1$ .

When point  $P$  on edge 12,  $L_3 = 0$ ; if it is on vertex 3, then  $L_3 = 1$ .

The major advantage of triangular elements is that they can be used in problems with irregular geometries. In finite element procedure, triangular mesh is widely adopted and area coordinates are used to represent both linear and nonlinear local functions.

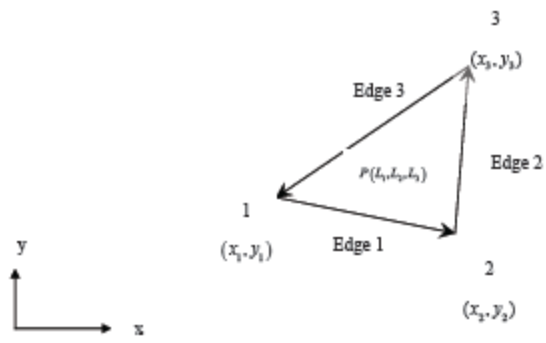


Figure 2.1. Parameters of a typical triangle

### 2.1.3 Linear interpolation function of magnetic potential

In a triangular element, the magnetic potential component  $A_z(x,y)$  at any point can be approximated by the linear interpolation function defined at every vertex.

In the triangle of Figure 2.1, the magnetic potential  $A_z(x,y)$  can be approximated as:

$$A(x, y) = a + bx + cy \quad (2.11)$$

If the potential has values of  $A_1$ ,  $A_2$  and  $A_3$ , and at the vertices 1, 2 and 3 respectively, then we apply Equation (2.11) to the three vertices to obtain,

$$\begin{cases} A_1 = a + bx_1 + cy_1 \\ A_2 = a + bx_2 + cy_2 \\ A_3 = a + bx_3 + cy_3 \end{cases} \quad (2.12)$$

This will allow us to solve for the expansion coefficients (a, b, c). The results are listed as follows,

$$\begin{cases} a = \frac{1}{2\Delta} (a_1 A_1 + a_2 A_2 + a_3 A_3) \\ b = \frac{1}{2\Delta} (b_1 A_1 + b_2 A_2 + b_3 A_3) \\ c = \frac{1}{2\Delta} (c_1 A_1 + c_2 A_2 + c_3 A_3) \end{cases} \quad (2.13)$$

Plugging Equation (2.13) in Equation (2.11), we get,

$$A(x, y) = \frac{1}{2\Delta} \sum_{i=1}^3 (a_i + b_i x + c_i y) A_i \quad (2.14)$$

In terms of area coordinates, Equation (2.14) becomes

$$A(x, y) = \sum_{i=1}^3 L_i A_i \quad (2.15)$$

Thus, we obtained the linear representation of the unknown potential using its values at the vertices of triangles.

### 2.1.4 Local element calculation

From Equation (2.15), nodal basis expansion in each element can be expected in such a form:

$$\vec{A}_z^e = \sum_{i=1}^3 C_i L_i(x, y) \hat{z} \quad \text{and} \quad \vec{A}_z^{oe} = \sum_{j=1}^3 L_j(x, y) \hat{z} \quad (2.16)$$

where  $C_i$  is the unknown coefficient which needs to be determined.

Now, we discretize Equation (2.5) on each triangle. The triangle index “e” is ignored for some quantities for simplicity. Define



$$S_{ij} = \int_V \frac{1}{\mu_r} (\nabla \times L_j(x, y) \hat{z}) \cdot (\nabla \times L_i(x, y) \hat{z}) dV \quad (2.17)$$

$$B_j = \int_V L_j(x, y) \hat{z} \cdot \vec{J}_z dV \quad (2.18)$$

$$\Gamma_{ij} = \int_V \frac{1}{\mu_r} L_j(x, y) \hat{z} \times (\nabla \times L_i(x, y) \hat{z}) \cdot \hat{n} dl \quad (2.19)$$

where  $\hat{n}$  denotes the unit vector normal to  $\Gamma$ .

Then, function  $F(\vec{A}_z^e, \vec{A}_z^{ae})$  can be expanded in local element as

$$F(\vec{A}_z^e, \vec{A}_z^{ae}) = \sum_{i=1}^3 \sum_{j=1}^3 (C_i S_{ij} - \mu_0 B_j - C_i \Gamma_j) \quad (2.20)$$

In the following part, we will discuss each matrix respectively.

### 1) S matrix calculation

Using some vector identities,  $S_{ij}$  can be simplified as

$$\begin{aligned} S_{ij} &= \int_V \frac{1}{\mu_r} (\nabla \times L_j(x, y) \hat{z}) \cdot (\nabla \times L_i(x, y) \hat{z}) dV \\ &= \int_V \frac{1}{\mu_r} \left( \frac{\partial}{\partial y} L_j \hat{x} - \frac{\partial}{\partial x} L_j \hat{y} \right) \cdot \left( \frac{\partial}{\partial y} L_i \hat{x} - \frac{\partial}{\partial x} L_i \hat{y} \right) dV \\ &= \int_V \frac{1}{\mu_r} \left( \frac{\partial}{\partial y} L_j \frac{\partial}{\partial y} L_i + \frac{\partial}{\partial x} L_j \frac{\partial}{\partial x} L_i \right) dV \end{aligned} \quad (2.21)$$

By the definition of area coordinates, the differential operation can be calculated as

$$\frac{\partial}{\partial y} L_i = \frac{\partial}{\partial y} \frac{a_i + b_i x + c_i y}{2\Delta} = \frac{1}{2\Delta} c_i \quad \text{and} \quad \frac{\partial}{\partial x} L_i = \frac{\partial}{\partial x} \frac{a_i + b_i x + c_i y}{2\Delta} = \frac{1}{2\Delta} b_i$$

In the same way, we have,

$$\frac{\partial}{\partial y} L_j = \frac{1}{2\Delta} c_j \quad \text{and} \quad \frac{\partial}{\partial x} L_j = \frac{1}{2\Delta} b_j$$

Imposing the results in equation (2.21),

$$\begin{aligned} S_{ij} &= \int_V \left( \frac{1}{2\Delta} c_i \frac{1}{2\Delta} c_j + \frac{1}{2\Delta} b_i \frac{1}{2\Delta} b_j \right) \frac{1}{\mu_r} dV \\ &= \int_{L_2=0}^1 \int_{L_1=0}^{1-L_2} \left( \frac{1}{2\Delta} c_i \frac{1}{2\Delta} c_j + \frac{1}{2\Delta} b_i \frac{1}{2\Delta} b_j \right) \frac{1}{\mu_r} \sqrt{g} dL_1 dL_2 \end{aligned}$$

where  $\sqrt{g} = 2\Delta$ , and  $\Delta$  is the area of the triangle

Then,

$$S_{ij} = \frac{1}{\mu_r} \left( \frac{1}{4\Delta} c_i c_j + \frac{1}{4\Delta} b_i b_j \right) \quad (2.22)$$

### 2) B matrix calculation

Similarly, the result of  $B$  matrix calculation can be written as

$$\begin{aligned}
B_J &= \int_V L_J(x, y) \hat{z} \cdot \vec{J}_z dV = J \int_V L_J dV \\
&= J \int_{L_2=0}^1 \int_{L_1=0}^{1-L_2} L_J \sqrt{g} dL_1 dL_2 \\
&= J \frac{1}{6} \sqrt{g} = J \frac{\Delta}{3}
\end{aligned}
\tag{2.23}$$

In the above, J is the excitation current at the center of the triangles.

### 3) matrix calculation $\Gamma$

By definition,

$$C_i \Gamma_y = \int_{\Gamma} \frac{1}{\mu_r} L_j(x, y) \hat{z} \times (\nabla \times C_i L_i(x, y) \hat{z}) \cdot \hat{n} dl$$

Using vector identities  $\nabla \times (ab) = a \nabla \times b - b \times \nabla a$ , and  $a \times (b \times c) = (a \cdot c)b - (a \cdot b)c$  we have,

$$\begin{aligned} \nabla \times (C_i L_i \hat{z}) &= C_i L_i (\nabla \times \hat{z}) - \hat{z} \times \nabla C_i L_i \\ &= C_i \nabla L_i \times \hat{z} \end{aligned} \quad (2.24)$$

Thus,

$$\begin{aligned} C_i \Gamma_y &= \int_{\Gamma} \frac{1}{\mu_r} L_j \hat{z} \times (C_i \nabla L_i \times \hat{z}) \cdot \hat{n} dl \\ &= \int_{\Gamma} \frac{1}{\mu_r} [(L_j \hat{z} \cdot \hat{z}) C_i \nabla L_i - (L_i \hat{z} \cdot C_i \nabla L_i)] \cdot \hat{n} dl \\ &= \int_{\Gamma} \frac{1}{\mu_r} L_j \nabla C_i L_i \cdot \hat{n} dl \end{aligned} \quad (2.25)$$

In the above, we have applied the fact the  $\nabla L$  is in x-y plane where  $\hat{z} \cdot \nabla L = 0$

For every triangular mesh,

$$\sum_{i=1}^3 C_i \Gamma_y = \int_{\Gamma} \frac{1}{\mu_r} L_j \frac{\partial A_z^e}{\partial n} dl \quad (2.26)$$

An example is given in Figure 2.2. Two adjacent triangular elements were used for illustration. In triangle 1,

$$\sum_{i=1}^3 C_i \Gamma_y = \frac{1}{\mu_r^{e1}} \frac{\partial A_z^{e1}}{\partial n} \left( \int_{\text{node1}}^{\text{node2}} L_j dl + \int_{\text{node2}}^{\text{node3}} L_j dl + \int_{\text{node3}}^{\text{node1}} L_j dl \right) \quad (2.27)$$

In triangle 2,

$$\sum_{i=1}^3 C_i \Gamma_y = \frac{1}{\mu_r^{e2}} \frac{\partial A_z^{e2}}{\partial n} \left( \int_{\text{node2}}^{\text{node4}} L_j dl + \int_{\text{node3}}^{\text{node2}} L_j dl + \int_{\text{node4}}^{\text{node3}} L_j dl \right) \quad (2.28)$$

For two adjacent triangle mesh which share a same edge, at the interface, the magnetic potential satisfies [12]

$$A_z^{e1} = A_z^{e2} \quad \text{and} \quad \frac{1}{\mu_r^{e1}} \frac{\partial A_z^{e1}}{\partial n} = \frac{1}{\mu_r^{e2}} \frac{\partial A_z^{e2}}{\partial n}$$

Thus, the middle terms of the right-hand side in Equation (2.27) and Equation (2.28) cancelled. Therefore,  $\Gamma$  matrix can be cancelled at all interior edges. We will discuss the outer boundary condition later.

#### 4) Magnetic flux density calculation

From Equation (2.1), B can be expanded in local element as,

$$\begin{aligned}
 B^e &= \sum_{i=1}^3 \nabla \times (C_i L_i) \hat{z} \\
 &= \sum_{i=1}^3 C_i \left( \frac{\partial}{\partial y} L_i \hat{x} - \frac{\partial}{\partial x} L_i \hat{y} \right) \\
 &= \sum_{i=1}^3 C_i \frac{1}{2\Delta} (c_i \hat{x} - b_i \hat{y})
 \end{aligned} \tag{2.29}$$

The weak form for local element Equation (2.20) can be simplified as:

$$F(\bar{A}_z^e, \bar{A}_z^{oe}) = \sum_{i=1}^3 \sum_{j=1}^3 (C_i S_{ij} - \mu_0 B_j) = C_{icm} S_{icm} - \mu_0 B_{icm}$$

To minimize the equation, we set  $\delta F = 0$ . This leads to

$$C_{icm} = \mu_0 B_{icm} S_{icm}^{-1}.$$

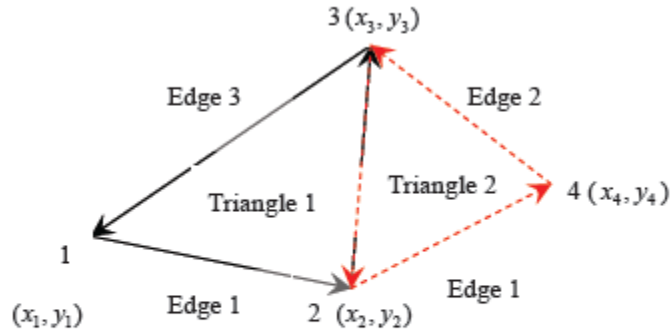


Figure 2.2. Example to illustrate the integration on the interior boundary

#### 2.1.5 Boundary Condition

There are several absorbing boundary conditions to be applied for mesh truncation. When the boundary is far enough to the transformer model, the Dirichlet Boundary Condition,

$$A(x, y) = 0 \tag{2.30}$$

on the outer boundary can yield an accurate solution.

## 2.2 Validation of finite element method

### 2.2.1 Ampere's circuital law

Ampere's circuital law states that the line integral of H about any closed path is exactly equal to the direct current enclosed by that path [14],

$$\oint H \cdot dL = I \quad (2.31)$$

The magnetic flux density is related to H by

$$B = \mu_0 \mu_r H \quad (2.32)$$

In the govern vector Poisson Equation  $\nabla \times \left( \frac{1}{\mu_r} \nabla \times \vec{A}_z \right) = \mu_0 \vec{J}_z$ ,  $\vec{J}_z$  denotes the electric current density with the unit A/m<sup>2</sup>. If  $\vec{J}_z$  is uniformly distributed, the total current I can be calculated from  $\vec{J}_z \cdot \Delta$ , where  $\Delta$  is the area containing  $\vec{J}_z$ .

We will test the FEM program with three test cases and compare the result with the exact H value computed by Ampere's circuital law.

### 2.2.2 Test case 1

The first case is a conductor of circular cross section with a radius  $a = 0.1\text{m}$  which has a relative permeability  $\mu_r = 1$ . A current density  $J = 1 \text{ A/m}^2$  is imposed on it. The background mesh is terminated at a circle of radius  $g = 1.2\text{m}$ . The geometry is shown in Figure 2.3.

The exact H can be calculated as

$$H = \frac{J\pi^2 r}{2\pi r} = \frac{J\pi}{2}, \quad r < a, \quad (2.33)$$

$$H = \frac{J\pi^2 a}{2\pi r} = \frac{J\pi a}{2r}, \quad r \geq a, \quad (2.34)$$

Using the finite element program, H is calculated at fixed angles of 0°, 45° and 90° respectively. Figure 2.4 is the comparison of results of FEM and the exact H value. Figure 2.5 and Figure 2.6 show the mesh plot [15]. The figures show that the results calculated by FEM agree well with the exact results.

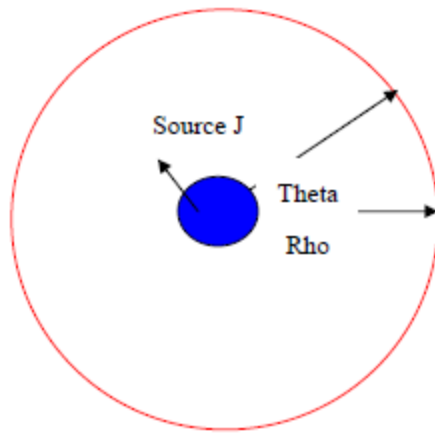


Figure 2.3. Case 1 geometric model

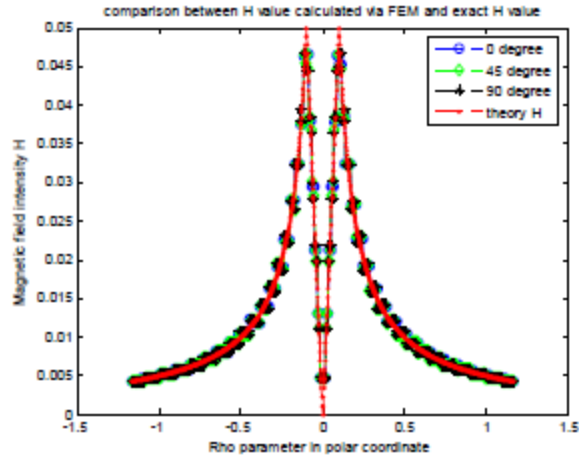


Figure 2.4. Comparison between H value calculated via FEM and exact result for Case 1

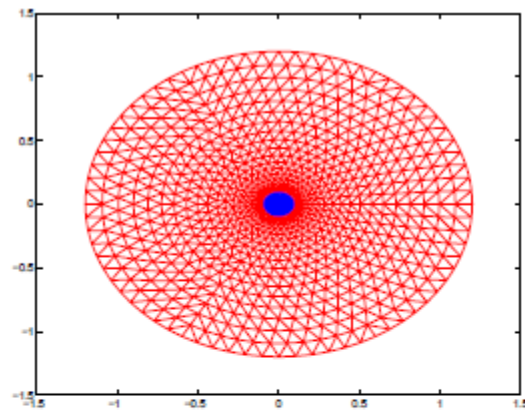


Figure 2.5. Mesh plot for Case 1

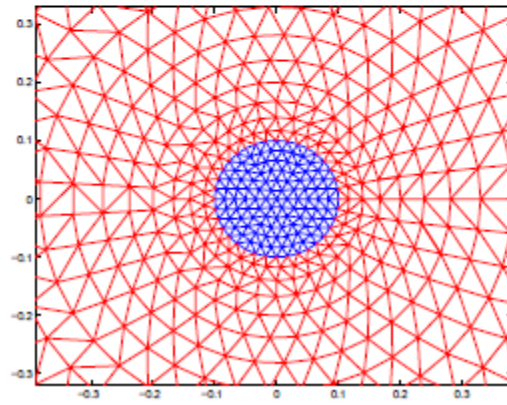


Figure 2.6. Detail mesh plot of Case 1



### 2.2.3 Test case 2

The second case is a circle cross section of a conductor with a radius which has a relative permeability  $\mu_r = 1$ . A current density  $J = 1 \text{ A/m}^2$  is imposed on it. A material which has a relative permeability  $\mu_r = 900$  surrounds the source with a radius  $b=0.2\text{m}$ . The background is filled of air with a radius  $g = 1\text{m}$  which has a relative permeability  $\mu_r = 1$ . The geometry is shown in Figure 2.7.

The exact H can be calculated in the same way as in case 1.

The finite element program calculated H at fixed angles of  $0^\circ$ ,  $45^\circ$  and  $90^\circ$  respectively. Figure 2.8 is the comparison of results of FEM and the exact H value.

Figure 2.9 and Figure 2.10 show the mesh plot.

The figures show that the results calculated by FEM agree well with the exact results

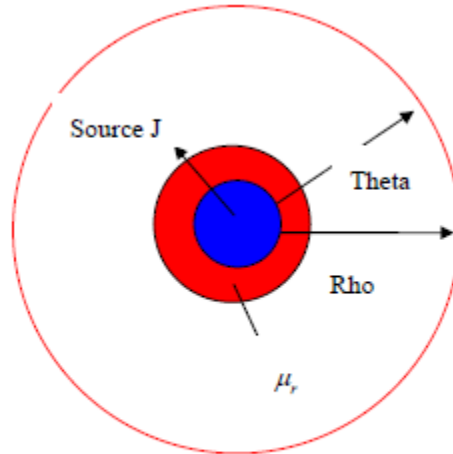


Figure 2.7. Geometric model of Case 2

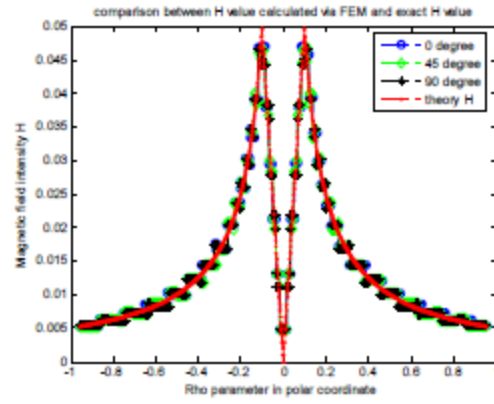


Figure 2.8. Comparison between H value calculated via FEM and exact H value in Case 2

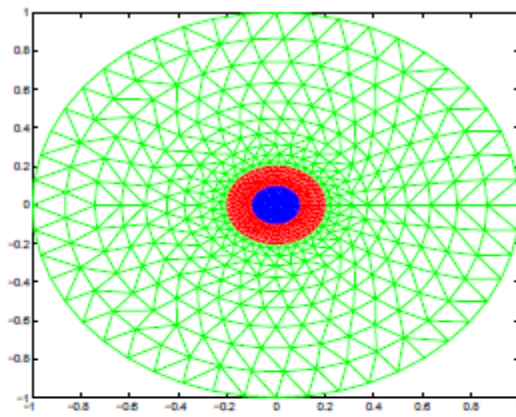


Figure 2.9. Mesh plot for Case 2

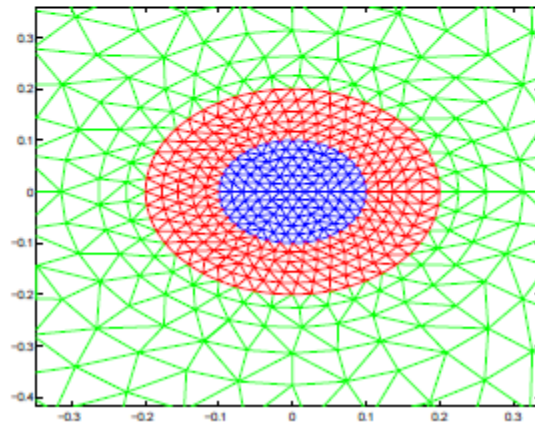


Figure 2.10. Detailed mesh plot for Case 2

### 2.2.4 Test case 3

The third case is a ring cross section of a conductor with an inner radius  $a = 0.1\text{m}$  and outer radius  $b = 0.2\text{m}$  which has a relative permeability  $\mu_r = 1$ . A current density  $J = 1 \text{ A/m}^2$  is imposed on it. A material which has a relative permeability  $\mu_r = 900$  surrounds the source with a radius  $c = 0.24\text{m}$ . The background is filled of air with a radius  $g = 1.2\text{m}$  which has a relative permeability  $\mu_r = 1$ . The geometry is shown in Figure 2.11.

The exact H can be calculated from

$$H = 0, \quad r < a, \quad (2.35)$$

$$H = \frac{\pi(r^2 - a^2)J}{2\pi r} = \frac{(r^2 - a^2)J}{2r}, \quad a \leq r < b, \quad (2.36)$$

$$H = \frac{\pi(b^2 - a^2)J}{2\pi r} = \frac{(b^2 - a^2)J}{2r}, \quad r \geq b, \quad (2.37)$$

The finite element program calculated H at fixed angles of  $0^\circ$ ,  $45^\circ$  and  $90^\circ$  respectively. Figure 2.12 is the comparison of results of FEM and the exact H value. Figure 2.13 and Figure 2.14 show the mesh plot.

From Figure 2.12, we can see that the results calculated via FEM match well with the exact results. Through testing three cases with regular geometry which have exact results, the algorithm and program of this 2D finite element method are demonstrated accurate to solve magnetostatic field. In the next section, this method will be applied on two models with different transformer core structures.

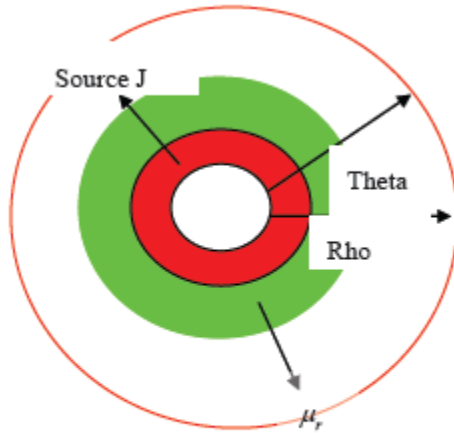


Figure 2.11. Geometric model of Case 3

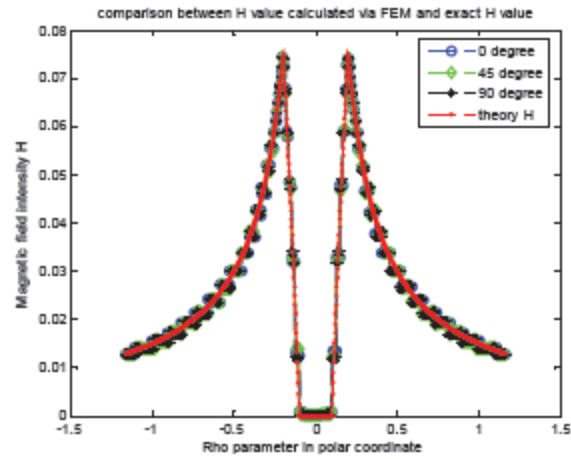


Figure 2.12. Comparison between H value calculated via FEM and exact H value in

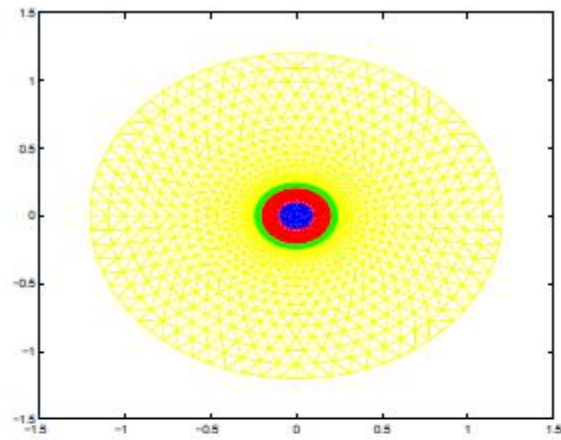


Figure 2.13. Mesh plot for Case 3

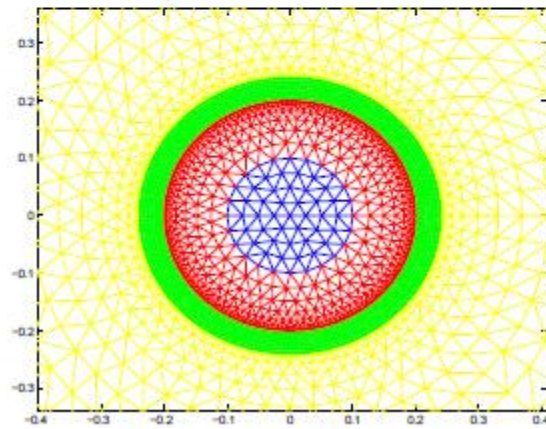


Figure 2.14. Detailed mesh plot for Case 3